

# Magnetomechanical design and power generation of magnetostrictive clad plate cantilever

Cite as: Appl. Phys. Lett. **115**, 243504 (2019); <https://doi.org/10.1063/1.5111351>

Submitted: 26 May 2019 . Accepted: 15 November 2019 . Published Online: 11 December 2019

Zhenjun Yang, Ryuichi Onodera, Tsuyoki Tayama, Masahito Watanabe, and Fumio Narita 



View Online



Export Citation



CrossMark

Lock-in Amplifiers  
up to 600 MHz



Zurich  
Instruments



# Magnetomechanical design and power generation of magnetostrictive clad plate cantilever

Cite as: Appl. Phys. Lett. **115**, 243504 (2019); doi: [10.1063/1.5111351](https://doi.org/10.1063/1.5111351)

Submitted: 26 May 2019 · Accepted: 15 November 2019 ·

Published Online: 11 December 2019



View Online



Export Citation



CrossMark

Zhenjun Yang,<sup>1</sup> Ryuichi Onodera,<sup>2</sup> Tsuyoki Tayama,<sup>2</sup> Masahito Watanabe,<sup>2</sup> and Fumio Narita<sup>1,a)</sup> 

## AFFILIATIONS

<sup>1</sup>Department of Materials Processing, Graduate School of Engineering, Tohoku University, Aoba-yama 6-6-02, Sendai 980-8579, Japan

<sup>2</sup>Research and Development Department, Tohoku Steel Co. Ltd., 23 Nishigaoka, Muratamachi, Shibatagun, Miyagi 989-1393, Japan

<sup>a)</sup>[narita@material.tohoku.ac.jp](mailto:narita@material.tohoku.ac.jp)

## ABSTRACT

A class of the magnetostrictive iron-cobalt/nickel clad plate cantilever is prepared in this study. The relevant ability for harvesting vibration energy is systematically investigated in comparison with the single iron-cobalt cantilever. In addition, the effects of the magnitude of bias magnetic field (i.e., external magnetic field) and the magnetization angle on the energy-harvesting performance are considered. The results indicated that the iron-cobalt/nickel clad plate cantilever exhibits far greater power generation compared with that of the single iron-cobalt cantilever. Besides, the iron-cobalt/nickel clad plate cantilever displayed high sensitivity to the magnitude of bias magnetic field and the magnetization angle. In more detail, the output voltage of the iron-cobalt/nickel clad plate cantilever peaks at a point even while the bias magnetic field constantly increases. A theory of dynamic balance can explain this phenomenon. Meanwhile, the resonance frequency of the iron-cobalt/nickel clad plate cantilever is proportional to the bias magnetic field due to the influence of the elastic modulus variation. This work provides insights into the exploration and design, not only of the vibration-energy-harvesting components but also of the sensitive detectors.

Published under license by AIP Publishing. <https://doi.org/10.1063/1.5111351>

Magnetostrictive materials have been attracting a great deal of consideration in sensors, actuators, and energy harvesters.<sup>1–3</sup> Because of its special characteristic in energy conversion, this kind of material has been widely studied as a magnetomechano-electric conversion component in self-powered microsystems, Internet of Things (IoT), and microdetectors.<sup>4,5</sup> In recent years, the performance of magnetostrictive materials in energy conversion obtains a great improvement through fabricating various magnetostrictive composites.<sup>6–8</sup>

Traditional magnetostrictive materials such as Terfenol-D, which has great magnetostriction, have been gaining noticeable attention for use in sensors. However, the extreme brittleness<sup>9,10</sup> hinders their further application, specifically in harvesting energy. To improve their mechanical properties, some researchers<sup>11,12</sup> have proposed methods for the preparation of different composites. These composites show a significant improvement in mechanical properties; however, this is at the expense of lower magnetostrictive properties. As a result, the harvesting performance has only a limited increase.<sup>13</sup> In addition, another alloying magnetostrictive material FeGa, namely, Galfenol alloy, exhibits considerable magnetostriction, making it a potential candidate. Nevertheless, the difficulty in machinability and the fabrication cost restrict its wide industrialization.<sup>14–16</sup> In addition

to these two dominant materials, certain materials such as amorphous Metglas and constituent FeCo exhibit excellent energy-harvesting ability.<sup>17–19</sup> In particular, the easy-producible FeCo alloy has a promising application in industrialization.

On the other hand, a consensus has been widely accepted that the bias magnetic field is essential for the magnetostrictive materials in energy conversion.<sup>20,21</sup> According to the characteristics of magnetostrictive materials, a bias magnetic field can rotate a domain or move a domain wall through changing the magnetic moment within the material, which then gives rise to an exterior shape change, and vice versa. During this process, the magnetomechanical energy conversion is realized. Furthermore, a pickup coil, enclosing the magnetostrictive material, is capable of generating electric energy through Faraday's law to eventually realize the magnetomechano-electric energy conversion. Although almost all the work has utilized the bias magnetic field, the effects of its detailed parameters (e.g., magnitude) on conversion efficiency were not clear.<sup>22,23</sup> In energy harvesting, based on the magnetostriction curve, there is generally an optimal value for the bias magnetic field, leading to maximum output. Thus, it is necessary to measure the variation of output power, for the bias magnetic field, in a changeable range instead of certain constant points. Besides, the easy

magnetization axis is usually employed for evaluating the ability of power generation, namely, in the  $d_{33}$  model.<sup>24</sup> However, in practical applications of magnetostrictive sensors or harvesters, the direction of the bias magnetic field often exhibits a slight deviation because of ambient influences such as vibration and movement. Moreover, the variation of magnetization or output power, in response to the magnetization angle, also provides possible uses in certain exterior magnetic or mechanical detectors. As a result, an investigation showing the relationship between output performance and magnetization angle could provide a theoretical basis and an experimental exploration in the design of relevant detecting components.

In this study, a class of the FeCo/Ni magnetostrictive clad plate cantilever is prepared. The power generation abilities of both the FeCo/Ni clad plate and single cantilevers are compared. This work is aimed at evaluating the design and performance of the magnetostrictive clad plate cantilever in harvesting energy. In addition, the effects of the magnitude and angle of the bias magnetic field on magnetization or power generation are systematically examined, specifically in the area of sensitivity. Therefore, this work offers practical and theoretical ideas regarding the design and application of detectors in detecting exterior magnetic and mechanic energy variations.

A class of iron-cobalt (FeCo)/nickel magnetostrictive clad plate cantilever was prepared in this work. Thermal diffusion bonding was employed to bond the FeCo and Ni sheets that had already undergone thermal and cold rolling. Following this, the FeCo/Ni clad plate was processed into the experimental cantilevers with dimensions of  $70 \times 5 \times 1$  mm. Here, a single FeCo cantilever was introduced to enable the characterization of the merits of the clad plate cantilever in harvesting vibration energy. The dimensions of the single FeCo cantilever are the same as those in FeCo/Ni clad plate cantilever. The physical assembly and schematic for harvesting vibration energy are illustrated in Fig. 1. The detailed properties of FeCo and Ni were shown in Table A1 and Fig. A1 (see the supplementary material). A proof mass of 5.1 g was positioned at the free end of the cantilevers to adjust the resonance frequency. A pickup coil with  $1 \times 10^5$  turns, a

resistance of  $119 \text{ k}\Omega$ , and a diameter of  $0.025 \text{ mm}$  encloses the magnetostrictive cantilever, where the effective power-generating part is approximately  $40 \text{ mm}$  in length, as shown in Fig. 1(c). A functional generator (GDS-3504, Good Will Instrument Co., Ltd.) was used to provide a sinusoidal signal which subsequently drove a bending vibration shaker (m030/MA1; IMV Corporation, Japan). Here, first, the output performance of the FeCo and FeCo/Ni cantilevers with respect to the input frequency was compared at a load resistance of  $119 \text{ k}\Omega$ . An exterior biasing magnet was employed to provide a powerful bias magnetic field in consideration of the relatively high saturated magnetization of the FeCo alloy.<sup>25</sup> Here, it must be emphasized that the bias magnetic field in this study represents the external magnetic field  $B_0$ . On the other hand, to examine the effects of the magnitude and angle of bias magnetic field, the extra coil windings (240 turns and the diameter of  $175 \text{ mm}$ ) instead of the magnet enclose the harvesting setup to offer a changeable bias magnetic field  $B_0$  in the range from  $0$  to  $7 \text{ mT}$  [Fig. 1(a)]. The energy harvesting setup here was under an opening electric circuit without any rectifier or load resistance. In particular, the harvesting setup was positioned on a removable stage, thus enabling the magnetization angle  $\theta$  to be changed, with the rotation of the stage, from  $0^\circ$  to  $80^\circ$ . The coordinates showing the relationship among every vector are illustrated in Fig. 1(b), with the  $z$ -axis being the axial direction along the length of the FeCo/Ni clad plate cantilever, namely, the easy axis to be magnetized. Here, the direction of bias magnetic field was assumed to be along the  $x_3$  direction. Thus, the angle between the  $z$  and  $x_3$  directions is referred to as the magnetization angle  $\theta$ .

The abilities for harvesting vibration energy between the FeCo/Ni clad plate cantilever and single FeCo cantilever were compared. To identify the optimal resonance frequency, Fig. 2 shows the correlation between the input frequency and the output voltage/power of these two cantilevers, (FeCo/Ni and single FeCo), in the range from  $40$  to  $60 \text{ Hz}$  at an amplitude of  $0.05 \text{ mm}$ . In this way, it indicated that the resonance frequency of FeCo/Ni was about  $50 \text{ Hz}$ . The input frequency of the single FeCo was adjusted to the same frequency of  $50 \text{ Hz}$ . From Fig. 2, the maximum output voltage and power of the FeCo/Ni clad plate cantilever are about  $29.77 \text{ V}$  and  $7.45 \text{ mW}$ , respectively. In contrast, the harvesting performance of the former is far greater than that of the single FeCo cantilever, by factors of approximately  $6.35$  and

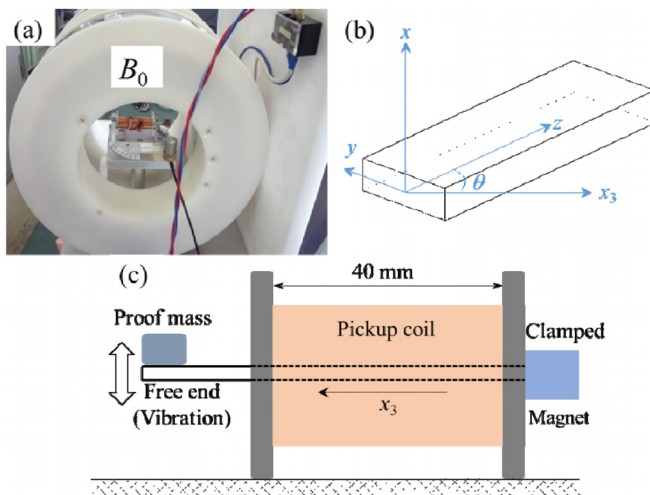


FIG. 1. (a) Physical assembly, (b) coordinates showing the vector directions, and (c) schematic for the experiment setup.

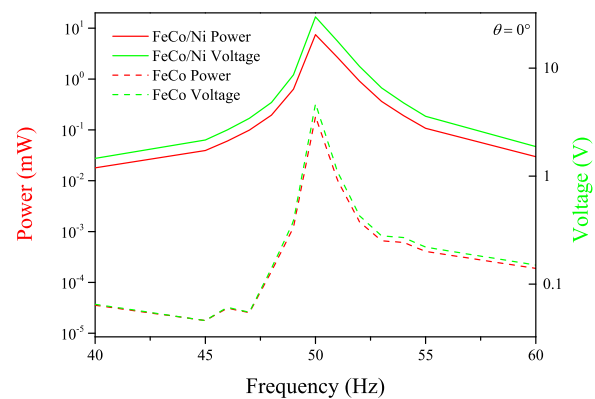


FIG. 2. Output powers and voltages as a function of the frequency of the FeCo/Ni clad plate and single FeCo cantilevers.

40.29, respectively. The corresponding mechanism is related to the different magnetostrictive properties of FeCo and Ni in response to the outside loadings (e.g., bias magnetic field or tension/compression). The details with respect to this phenomenon have been previously reported.<sup>26</sup>

To determine the effects of the magnitude of the bias magnetic field for the FeCo/Ni clad plate cantilever on harvesting efficiency, the extra coil windings ( $B_0$ ) were used to excite a changeable bias magnetic field. These results, as shown in Fig. 3, reveal the relationship between voltage, bias magnetic field, and resonance frequency. At first, the curves of the output voltage, at every frequency, show an upward tendency at the start with increasing bias magnetic field and then reach a peak. Following this, there is an obvious fall in the value of the output voltage. This is more relatively accurate in comparison to other results that examined the harvesting performance at certain points only. In particular, the results in this study clearly indicate that the output voltage has a maximum value with the increasing bias magnetic field. This reason is related to the magnetic induction variation in response to bending vibration. Namely, the magnetic induction variation exhibits a maximum at one point during this process. This phenomenon is attributed to the dynamic balance between the stress and the bias magnetic field in terms of magnetic domain rotation and wall motion. First, the stress resulting from bending and the bias magnetic field alternates as the dominant factor that drives the rotation of the domain. Consequently, there is a dynamic balance around a position to control the rotation of domain. Figure 4 shows a schematic illustrating this transformation for the rotation of the domain. In more detail, this process depicts the rotation of domain, undergoing the increasing stress, within several domain grains. It is assumed that the model is a common  $d_{33}$  model, namely, the direction of stress is parallel to that of the bias magnetic field. When the bias magnetic field is dominant, it forces the magnetic induction vector to align in the same direction, as shown in Fig. 4(a). In this way, even though the stress or bias magnetic field varies, the domain is only able to rotate in a relatively minor angle on one side of the initial position [see Fig. 4(d)]. In contrast, when the stress is the dominant factor affecting the rotation, the arrows showing the magnetic induction vector are always perpendicular to bias magnetic field [see Fig. 4(c)]. Similarly, the rotation of the domain is also constrained, so restricting its movement to one side of the initial

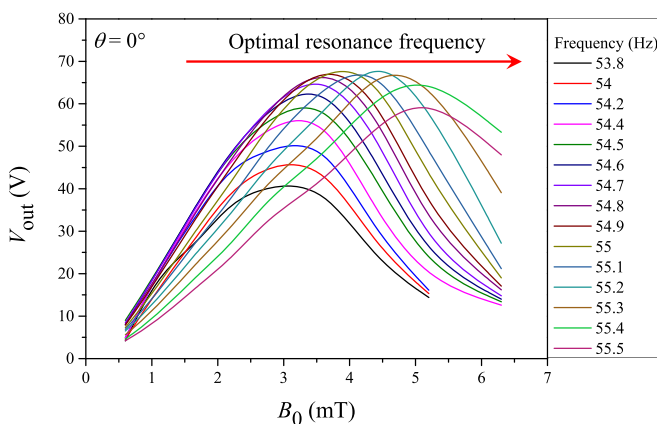


FIG. 3. Output voltage as a function of the bias magnetic field and resonance frequency.

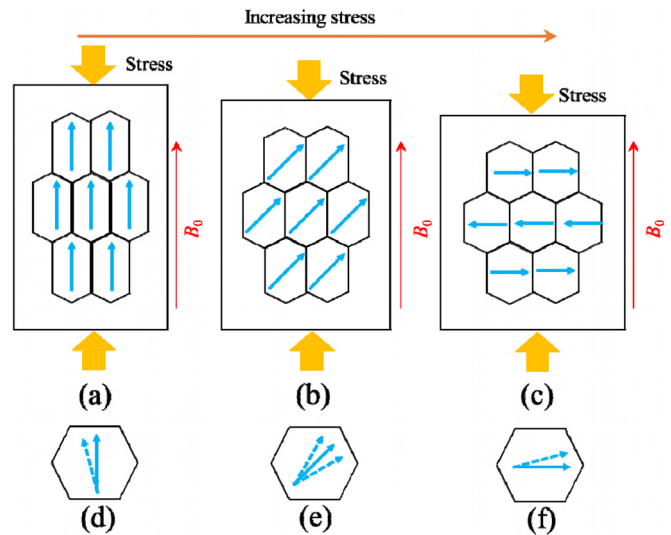
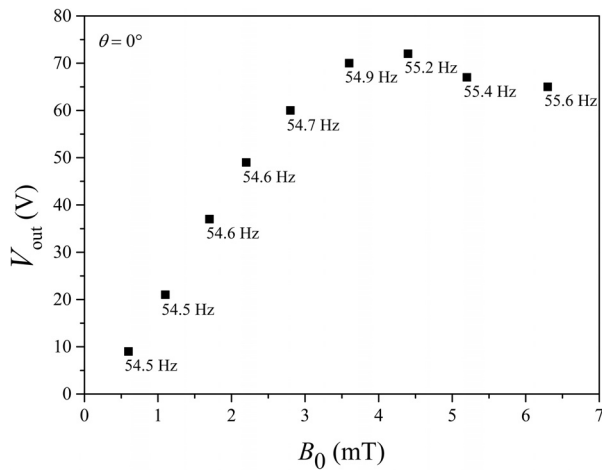


FIG. 4. Schematic for the rotation of domain related to the bias magnetic field and stress.

position only [see Fig. 4(f)]. However, Fig. 4(b) indicates a so-called dynamic balance between the stress and the magnetic bias field, which differs from the previous two situations. Here, because these two parameters are in a dynamic balance, the rotation of the magnetic domain can move toward either side of the initial position (i.e., dynamic balance point), see Fig. 4(e). Thus, the rotation of the domain, in this dynamic balance, exhibits a relatively wide angle which results in a great variation of magnetic induction and the great output voltage. On the other hand, both stress and magnetization can lead to motion for the magnetic domain wall. In general, this motion for the magnetic domain wall is clarified into two types: reversible and irreversible. Of those, the irreversible motion is referred to as the Barkhausen jumps, which always gives rise to a larger variation in magnetic induction. As a result, the dynamic balance between the stress and the bias magnetic field leads to the specimens to be at a critical point of the reversible and irreversible motion for the magnetic domain wall. When the stress and/or the bias magnetic field change, there is a considerable variation in magnetic induction, which leads to the peak of the output voltage. In conclusion, the reason for the observed peak of the output voltage is attributed to the particular dynamic balance of the stress and the bias magnetic field, where it generates greater magnetic induction variation during the bending vibration. This is why some researchers<sup>27</sup> reported that a prestress has the benefits of exciting greater output performance at a constant bias magnetic field (see the [supplementary material](#)).

On the other hand, Fig. 3 also indicates that the resonance frequency is proportional to the bias magnetic field. It is not difficult to conclude that there is an optimal resonance frequency at every bias magnetic field. It seems that there is a correlation between these two parameters. In order to clearly understand the relevant mechanism, the optimal resonance frequency at every bias magnetic field is presented in Fig. 5. It is evident that the resonance frequency rises with increasing bias magnetic field. This phenomenon can be explained through the inherent characteristics of magnetostrictive materials.



**FIG. 5.** Variations of the output voltage and resonance frequency with increasing bias magnetic field.

Differing from traditional materials, the magnetostrictive materials involve two kinds of deformation during bending vibration in a bias magnetic field. They are referred to as common elastic strain and magnetostrictive strain. In addition, the magnetostrictive strain is not proportional to the bias magnetic field. Therefore, the practical elastic modulus with respect to the strain is a variable such that the resonance frequency, corresponding to elastic modulus, differs with the increasing bias magnetic field. Although the resonance frequency at every bias magnetic field is different, there is an optimal combination such that the output voltage has a maximum value at a frequency of 55.2 Hz and a bias magnetic field of approximately 4.5 mT. In consideration of the polycrystallinity of the FeCo/Ni clad plate cantilever, it is reasonable to assume that the cantilever is in the state of the aforementioned, dynamic balance in this situation during the bending vibration.

The effects of magnetization angle  $\theta$  on power generation for the FeCo/Ni clad plate cantilever were also investigated in the range from  $0^\circ$  to  $80^\circ$ . Figure 6 reveals that the curves of the output voltage for the

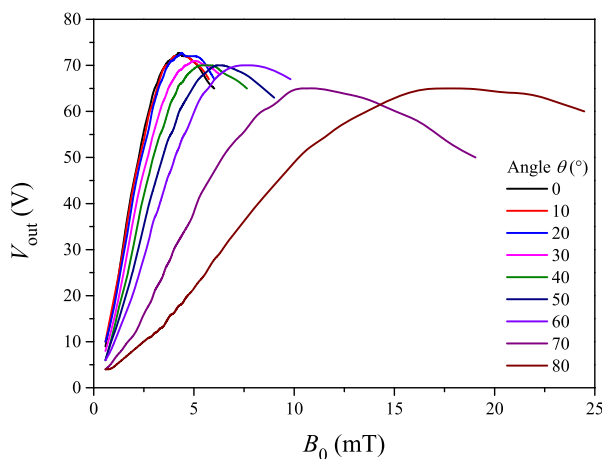


**FIG. 6.** Variation of the output voltage of the FeCo/Ni clad plate cantilever with the increasing magnetization angle.

FeCo/Ni cantilever at every angle differ with the increasing bias magnetic field. Of these, the curve of the output voltage for every angle reaches a peak before showing a downward tendency, which is attributed to the theory of dynamic balance as described above. In addition to that, there is another feature that the width of every curve broadens with the increasing bias magnetic field. It indicates that the sensitivity to the bias magnetic field, for the FeCo/Ni clad plate cantilever, slightly reduces with the increasing magnetization angle. Besides, the maximum output voltage, at every angle, declines with the increasing magnetization angle, owing to the characteristic of demagnetization within the FeCo/Ni clad plate cantilever. In general, the demagnetization is only related to the shape factor. The effects of demagnetization can be omitted when the length (i.e., magnetization direction) is far greater than the width of the magnetostrictive materials. However, due to the decreasing ratio of the length and width in the magnetization direction, the demagnetization has to be considered. As a result, the changeable magnitude of the magnetic induction, in response to the bending vibration, reduces because of the cancelation of the magnetization and demagnetization within the FeCo/Ni clad plate cantilever which then leads to the decrease in the output voltage. To characterize the difference in the maximum output voltage at every angle, the relevant comparison is exhibited in Fig. 7. It reveals that the output voltage has an obvious reduction when the magnetization angle ranges from  $20^\circ$  to  $30^\circ$ , and from  $60^\circ$  to  $70^\circ$ . In addition, the corresponding optimal bias magnetic field is proportional to the magnetization angle. These findings are mostly attributed to the effects of demagnetization. According to the theory of the magnetic domain, to maintain the systematical energy conservation, the magnetic domain is categorized to the removable domain and immovable domain. Of these, the demagnetization is the crucial factor responsible for the transformation between removable domain and immovable domain. From Fig. 7, the reducing curve of the output voltage is attributed to the transformation from the removable domain to the immovable domain even with the increasing bias magnetic field. Besides, there is also a staged response in output voltage which reveals that the increasing bias magnetic field is capable of offsetting the effect of the demagnetization and then maintaining the similar output voltage. On the other hand, it can be found that the variations both of both the output voltage and

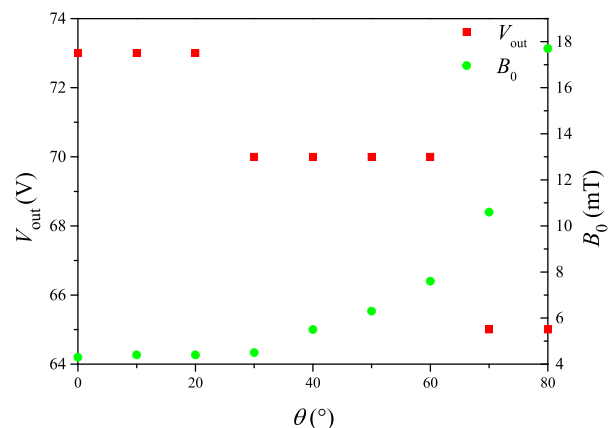


**FIG. 7.** Maximum output voltage of the FeCo/Ni clad plate cantilever as a function of the bias magnetic and the magnetization angle.



bias magnetic field are significant with the increasing magnetization angle. This provides the possibility of designing a class of sensitive detectors that examines the variation of the output voltage through the adjustment of exterior parameters, such as bias magnetic field and magnetization angle.

A type of the FeCo/Ni clad plate cantilever is studied in this work, and the corresponding feasibility of harvesting vibration energy is systematically investigated in comparison to the single FeCo cantilever. The results indicate that the energy-harvesting ability of the FeCo/Ni clad plate cantilever is far greater than that of the single FeCo cantilever because of the enhancement in magnetic induction variation between FeCo, with positive magnetostriction, and Ni with negative magnetostriction in response to the bending vibration. In addition, the output voltage of the FeCo/Ni clad plate cantilever peaks at a point while the bias magnetic field constantly increases. Furthermore, the resonance frequency of the FeCo/Ni clad plate cantilever is proportional to the bias magnetic field owing to the variation of elastic modulus stemming from the magnetostriction. On the other hand, the output voltage of the FeCo/Ni clad plate cantilever is inversely proportional to the magnetization angle. In conclusion, this work provides insights into the exploration and design, not only of the vibration-energy-harvesting components but also of the sensitive detectors.

See the [supplementary material](#) for the material properties and the theoretical model.

## REFERENCES

- <sup>1</sup>M. Radgolchin and H. Moenfarid, *Smart Mater. Struct.* **27**, 025015 (2018).
- <sup>2</sup>C. C. Jin, X. C. Liu, C. H. Liu, Y. Wang, H. L. Hwang, and Q. Wang, *Mater. Des.* **144**, 55–63 (2018).
- <sup>3</sup>M. Ito, K. Kamada, A. Yoshikawa, T. Kawamata, S. Fujieda, S. Suzuki, T. Minamitani, and T. Ueno, *J. Alloys Compd.* **731**, 898–902 (2018).
- <sup>4</sup>Y. J. Han, H. Wang, T. L. Zhang, Y. K. He, and C. B. Jiang, *Appl. Phys. Lett.* **112**, 082402 (2018).
- <sup>5</sup>G. Youssef, M. Lopez, and S. Newacheck, *Smart Mater. Struct.* **26**, 037003 (2017).
- <sup>6</sup>M. C. Wong, L. Chen, G. X. Bai, L. B. Huang, and J. H. Hao, *Adv. Mater.* **29**, 1701945 (2017).
- <sup>7</sup>L. Jin, W. L. Deng, Y. C. Su, Z. Xu, H. Meng, B. Wang, H. P. Zhang, B. B. Zhang, L. Zhang, X. B. Xiao, M. H. Zhu, and W. Q. Yang, *Nano Energy* **38**, 185–192 (2017).
- <sup>8</sup>A. Yoffe and D. Shilo, *Smart Mater. Struct.* **26**, 065007 (2017).
- <sup>9</sup>M. Peron, K. Katabira, L. M. Viespoli, F. Narita, and F. Berto, *Theor. Appl. Fract. Mech.* **99**, 194–204 (2019).
- <sup>10</sup>M. Colussi, F. Berto, and F. Narita, *Adv. Eng. Mater.* **18**, 2063–2069 (2016).
- <sup>11</sup>B. Ozkale, N. Shamsudhin, T. Bugmann, B. J. Nelson, and S. Pane, *Electrochem. Commun.* **76**, 15–19 (2017).
- <sup>12</sup>L. Chen, P. Li, Y. Wen, and Y. Zhu, *Compos. Struct.* **119**, 685–692 (2015).
- <sup>13</sup>Z. X. Deng and M. J. Dapino, *Smart Mater. Struct.* **26**, 103001 (2017).
- <sup>14</sup>N. L. Raveendran, R. Pandian, S. Murugesan, K. Asokan, and R. T. R. Kumar, *J. Alloys Compd.* **704**, 420–424 (2017).
- <sup>15</sup>V. V. Palacheva, A. Emdadi, F. Emeis, I. A. Bobrikov, A. M. Balagurov, S. V. Divinski, G. Wilde, and I. S. Golovin, *Acta Mater.* **130**, 229–239 (2017).
- <sup>16</sup>Z. X. Deng and M. J. Dapino, *Smart Mater. Struct.* **26**, 055027 (2017).
- <sup>17</sup>X. H. Ge, H. Ji, Y. Li, J. K. Chen, and Y. G. Wang, *J. Alloys Compd.* **752**, 303–307 (2018).
- <sup>18</sup>W. Wang, Y. N. Jia, X. F. Xue, Y. Liang, and Z. F. Du, *Smart Mater. Struct.* **27**, 105040 (2018).
- <sup>19</sup>F. Narita, *Adv. Eng. Mater.* **19**, 1600586 (2017).
- <sup>20</sup>X. P. Xu, C. L. Zhang, Q. K. Han, and F. L. Chu, *Appl. Phys. Lett.* **113**, 013901 (2018).
- <sup>21</sup>C. D. Pham, J. Chang, M. A. Zurbuchen, and J. P. Chang, *ACS Appl. Mater. Interfaces* **9**, 36980–36988 (2017).
- <sup>22</sup>M. M. Li, J. H. Li, X. Q. Bao, X. Mu, and X. X. Gao, *Mater. Des.* **135**, 197–203 (2017).
- <sup>23</sup>K. Katabira, Y. Yoshida, A. Masuda, A. Watanabe, and F. Narita, *Materials* **11**, 406 (2018).
- <sup>24</sup>Z. J. Yang, H. Kurita, R. Onodera, T. Tayama, D. Chiba, and F. Narita, *Smart Mater. Struct.* **28**, 034001 (2019).
- <sup>25</sup>F. Narita and M. Fox, *Adv. Eng. Mater.* **20**, 1700743 (2018).
- <sup>26</sup>Z. J. Yang, K. Nakajima, R. Onodera, T. Tayama, D. Chiba, and F. Narita, *Appl. Phys. Lett.* **112**, 073902 (2018).
- <sup>27</sup>C. M. Leung, J. F. Li, D. Viehland, and X. Zhuang, *J. Phys. D: Appl. Phys.* **51**, 263002 (2018).